

# Model Study of Eigen-Microstate Signatures of Criticality in Relativistic Heavy-Ion Collisions

Ranran Guo,<sup>1</sup> Jin Wu,<sup>2</sup> Mingmei Xu,<sup>1,\*</sup> Zhiming Li,<sup>1</sup> Zhengning Yin,<sup>1</sup> Yufu Lin,<sup>3</sup> Lizhu Chen,<sup>4</sup> Yanhua Zhang,<sup>5</sup> Jinghua Fu,<sup>1</sup> Xiaosong Chen,<sup>6,7</sup> and Yuanfang Wu<sup>1,†</sup>

<sup>1</sup>*Key Laboratory of Quark and Lepton Physics (MOE) and Institute of Particle Physics, Central China Normal University, Wuhan 430079, China*

<sup>2</sup>*College of Physics and Electronic Information Engineering, Guilin University of Technology, Guilin 541004, Guangxi, China*

<sup>3</sup>*College of Physics and Technology, Guangxi Normal University, Guilin 541004, Guangxi, China*

<sup>4</sup>*School of Physics and Optoelectronic Engineering,*

*Nanjing University of Information Science and Technology, Nanjing 210044, China*

<sup>5</sup>*Department of Physics and Electronic Engineering,*

*Yuncheng University, Yuncheng 044000, Shanxi, China*

<sup>6</sup>*Institute for Advanced Study in Physics, Zhejiang University, Hangzhou 310058, China*

<sup>7</sup>*School of Systems Science and Institute of Nonequilibrium Systems,*

*Beijing Normal University, Beijing 100875, China*

(Dated: February 3, 2026)

We present a comprehensive model study of the eigen-microstate approach (EMA) for identifying critical fluctuations in relativistic heavy-ion collisions. Using UrQMD and two stochastic baseline models, we demonstrate that EMA is insensitive to conventional short-range correlations and effectively filters out non-critical backgrounds. Critical fluctuations embedded via event-level or particle-level replacement with CMC events generate characteristic cluster-like eigen-microstate patterns and enhanced leading eigenvalues, with event-level criticality producing stronger responses. The eigen microstates exhibit the same pattern across different scales, demonstrating that the fractal nature of critical fluctuations is captured by the eigen microstates. Finite-size scaling of eigenvalue ratios exhibits fixed-point behavior, confirming the largest eigenvalue as an effective order-parameter-like quantity. These results demonstrate that EMA offers a robust and background-independent method for critical-point searches in the RHIC Beam Energy Scan and future heavy-ion experiments.

PACS numbers:

## I. INTRODUCTION

Mapping the phase structure of Quantum Chromodynamics (QCD), in particular locating the conjectured QCD critical point (CP), remains a central goal in contemporary nuclear physics [1]. Lattice QCD calculations at a small baryon chemical potential suggest a smooth crossover [2], while many effective models predict a first-order phase transition at higher baryon density [3, 4] terminating at a second-order CP [5, 6]. Experimental confirmation of such a CP would have profound implications for our understanding of strongly interacting matter and the nature of the QCD phase transition.

The search for CP has been a major focus of the RHIC Beam Energy Scan (BES) program [7] and will continue at FAIR, NICA, and HIRFL-CSR. A wide variety of observables have been proposed to capture the enhanced fluctuations and long-range correlations expected near the CP. These include higher-order cumulants of conserved charges [6, 8], factorial moments and intermit-

tency exponents of multiplicity distributions [9, 10], various two- and multi-particle correlation functions [11]. Despite extensive effort over more than two decades, clear and unambiguous evidence of a QCD CP has not yet been found [12].

One major difficulty is that existing observables are strongly affected by non-critical backgrounds: resonance decays, global conservation laws, hadronic rescatterings, collective flow, detector acceptance, finite-size effects, and so on. In addition, heavy-ion collisions are short-lived, rapidly expanding, and intrinsically dynamical systems. The degree of equilibration is uncertain [13–17], and the genuine thermodynamic order parameter is not directly accessible via the final-state hadrons. Many proposed signatures also require very high statistics [7, 18, 19], especially higher-order cumulants. These issues complicate the extraction of small critical contributions from large non-critical backgrounds.

These challenges motivate the development of new methods that can isolate the predominate critical mode from event-by-event data, while minimizing reliance on equilibrium assumptions or explicit background subtraction. The eigen-microstate approach (EMA) has recently been proposed as such a framework [20–24]. Instead of constructing a particular fluctuation observable, the

\*Electronic address: xumm@ccnu.edu.cn

†Electronic address: wuyf@ccnu.edu.cn

EMA regards each event as a microstate and analyzes the ensemble by diagonalizing an event–event correlation matrix. The resulting eigen microstates (EMs) provide a natural decomposition into collective modes, and “the condensation” of the leading eigenvalue signals the dominance of a collective pattern in the ensemble.

In previous work, EMA has been successfully applied to a range of systems, including equilibrium spin models [20, 21] (as well as previous Principal Component Analysis [25]), nonequilibrium living systems [22], vortex streets [23] and atmospheric and social dynamics, where it has been shown to reveal critical patterns and extract order-parameter-like quantities without relying on equilibrium thermodynamics. Recently, EMA has been applied to relativistic heavy-ion collisions using Ultra-relativistic Quantum Molecular Dynamics (UrQMD) and Critical Monte Carlo (CMC) simulations, demonstrating that the leading eigenvalue behaves as a robust order-parameter-like quantity and that its associated EMs exhibit a distinctive critical pattern [26].

The purpose of the present work is to perform a detailed and systematic model study of EMA in the context of relativistic heavy-ion collisions and to clarify its sensitivity to different classes of correlations. First, by comparing UrQMD and two stochastic baseline models, we show that EMA is largely insensitive to conventional short-range correlations and only responds to the average kinetic constraints shared by all events. Second, by superimposing critical fluctuations from CMC via both event-level and particle-level hybrid constructions, we study how cluster-like EM patterns emerge with increasing critical fraction and how the largest eigenvalue behaves as an order-parameter-like indicator. Finally, we investigate finite-size scaling of both EM patterns and eigenvalue ratios and identify fixed-point behavior at matching critical fractions, providing further evidence that EMA captures genuine critical scaling.

These results provide direct guidance for the application of EMA to experimental data from RHIC BES II and future relativistic heavy-ion programs and highlight its potential as a background-filtering tool for critical-point searches.

The paper is organized as follows: Section II introduces the EMA in relativistic heavy-ion collisions. The EMs and cumulative eigenvalue weights for non-critical models, including UrQMD and two stochastic baseline models, are given in Section III. Critical patterns of EMs for hybrid models with critical fluctuations are shown in Section IV. Section V discusses the finite-size scaling behavior of both critical patterns and eigenvalue ratios. Section VI provides a summary and conclusions.

## II. THE EIGEN-MICROSTATE APPROACH

In relativistic heavy-ion collisions, the experimentally accessible observables are the phase-space distributions of final-state charged particles. Even under identical

macroscopic conditions—collision energy, nuclear species, and impact parameter—the final-state particle distributions fluctuate significantly from event to event. These variations arise from differences in the dynamical evolution of each collision. When a quark-gluon plasma forms, distinct evolution paths correspond to different times of chemical and kinetic freeze-out. Consequently, each event can be considered a specific original microstate (OM) that encapsulates a unique temporal sequence of evolution, similar to that in the Ising model [17].

For the EMA in relativistic heavy-ion collisions [26], we simply focus on fluctuations of final-state charged particles in transverse-momentum space. The  $(p_x, p_y)$  plane is discretized into  $N = L \times L$  square bins. For the  $i$ -th event, the corresponding original microstate can be defined by a vector of the multiplicity fluctuations in overall bins of transverse-momentum space,

$$x_k^i = \Delta N_{\text{ch},k}^i = N_{\text{ch},k}^i - \langle N_{\text{ch},k} \rangle, \quad k = 1, \dots, N; \quad i = 1, \dots, M, \quad (1)$$

where  $N_{\text{ch},k}^i$  is the number of charged particles in the bin  $k$  in the event  $i$ , and  $\langle N_{\text{ch},k} \rangle$  denotes the multiplicity averaged by events in the bin  $k$ .

From the ensemble of  $M$  events, we construct the event-event (temporal-space) correlation matrix

$$C_{ij} = \frac{1}{\mathcal{N}} \sum_{k=1}^N x_k^i x_k^j, \quad (2)$$

which is real and symmetric.  $\mathcal{N} = \sum_{i=1}^M \sum_{k=1}^N (x_k^i)^2$ . Diagonalizing  $C$  yields eigenvalues  $\lambda_n$  and the corresponding linear independent eigenvectors  $\mathbf{v}^{(n)}$ ,

$$\sum_{j=1}^M C_{ij} v_j^{(n)} = \lambda_n v_i^{(n)}, \quad n = 1, \dots, M. \quad (3)$$

The eigenvalues are ordered as  $\lambda_1 \geq \lambda_2 \geq \dots \geq \lambda_M$ .

The  $n$ -th eigen-microstate ( $\mathbf{EM}_n$ ) is constructed as a linear combination of event microstates,

$$\mathbf{EM}_n = \sum_{i=1}^M v_i^{(n)} \mathbf{x}^i. \quad (4)$$

Its squared norm equals the eigenvalue,

$$|\mathbf{EM}_n|^2 = \lambda_n. \quad (5)$$

Therefore, the eigenvalues themselves can be interpreted as the statistical weights of the corresponding EMs, i.e.  $w_n = \lambda_n$ . The weights satisfy normalization as

$$\sum_{n=1}^M w_n = 1, \quad (6)$$

due to the choice of  $\mathcal{N}$ .

In the limit  $M \rightarrow \infty$ , if the largest weight  $w_1$  becomes finite, a condensation-like phenomenon is expected: a

leading eigenvalue  $\lambda_1$  becomes significantly larger than subleading eigenvalues, and the corresponding EM develops a coherent cluster or patch-like structure. This condensation is similar to the Bose-Einstein condensation [27]. The weight  $w_1$  therefore plays the role of an order parameter [20–25]. Both the emergence of a dominant weight and the appearance of a structured EM provide signatures of criticality.

The note is that each eigenvector is defined only up to an overall sign. Transformation  $\mathbf{v}^{(n)} \rightarrow -\mathbf{v}^{(n)}$ , leaves the equation and the eigenvalue  $\lambda_n$  unchanged, but flips the sign of the corresponding EM. Therefore, the overall sign of an EM has no physical meaning. The physically relevant information lies in the spatial shape, localization, and relative amplitude of the EMs and in the hierarchy of their weights.

The cumulative weight is defined as

$$C(m) = \sum_{n=1}^m w_n, \quad (7)$$

where  $m$  is the number of eigenvalues.  $C(m)$  provides the speed of the weight going to saturated value 1. The faster the speed to saturation, the more order the system is, cf., that of the temperature from above to below the critical one in the Ising model [20].

### III. EIGEN-MICROSTATES OF NON-CRITICAL MODELS

To understand how conventional dynamical correlations influence the eigenvalue spectra and EM patterns, we first study non-critical reference systems. We consider UrQMD, and two stochastic models that share the same event-by-event multiplicity distribution as that of UrQMD, but differ in whether they impose global kinetic constraints. In the following analysis, each ensemble contains  $M = 20,000$  events.

#### A. UrQMD baseline

As a realistic non-critical baseline, the cascade mode of UrQMD model [28, 29] is used. We generate 0–5% most-central Au+Au collisions at  $\sqrt{s_{\text{NN}}} = 19.6$  GeV using UrQMD (v3.4). Final-state charged particles are selected within the STAR acceptance of high moment analysis [12, 30]:

- pseudorapidity  $|\eta| < 0.5$ ,
- transverse momentum windows

$$0.2 < p_t < 1.6 \text{ GeV}/c \text{ for } \pi^\pm \text{ and } K^\pm,$$

$$0.4 < p_t < 2.0 \text{ GeV}/c \text{ for } p \text{ and } \bar{p}.$$

These cuts define the baseline event ensemble and are applied to all model and hybrid samples analyzed in this work.

UrQMD incorporates essential non-critical dynamics of heavy-ion collisions, including energy–momentum and charge conservation, resonance production and decay, hadronic rescatterings, and collective flow. We will examine to what extent these conventional mechanisms leave an imprint on the EM patterns.

#### B. Stochastic models with and without kinetic constraints

To separate the influence of global spectral shapes from that of true dynamical correlations, we construct two stochastic reference ensembles:

- **Stochastic model I without kinetic constraints.** In each event, the total charged multiplicity is drawn from the same multiplicity distribution as UrQMD. The particle momenta are then assigned independently and uniformly in  $p_x, p_y \in (-1, 1)$  GeV/ $c$ . No azimuthal modulation or transverse-momentum structure is imposed; this ensemble contains no inter-particle correlations and no common momentum shape.
- **Stochastic model II with kinetic constraints.** Events again share the UrQMD multiplicity distribution, but transverse momenta of the particle  $p_t$  are drawn from the global momentum distribution  $p(p_t) = \frac{1}{\Gamma(k) \beta^k} p_t^{k-1} e^{-p_t/\beta}$  where  $\Gamma(k)$  is the Gamma function,  $k$  and  $\beta$  are parameters which are obtained by fitting the  $p_t$  spectrum of UrQMD samples. The azimuthal angle  $\phi$  is sampled from a weakly anisotropic flow-modulated distribution  $p(\phi) = \frac{1}{2\pi} (1 + 0.08 \cos 2\phi)$ . These constraints impose a global momentum-shape structure (a realistic  $p_t$  spectrum and small elliptic-flow-like modulation) but do not introduce any intrinsic particle–particle correlations.

These two stochastic ensembles thus provide clean baselines “without” and “with” kinetic constraints, allowing us to isolate the role of global momentum shapes from that of UrQMD-specific dynamical correlations.

#### C. Eigen-microstate patterns and eigenvalue cumulants

Figure 1 displays the first three EMs ( $\text{EM}_1$ ,  $\text{EM}_2$ ,  $\text{EM}_3$ ) for UrQMD and the two stochastic reference models. Each EM is shown as a color map in the  $(p_x, p_y)$  plane. Red and blue denote positive and negative values of  $\Delta N_{\text{ch}}$ . Several non-critical features are evident:

- $\text{EM}_1$  is essentially *identically colored* for all three ensembles. Because the overall sign of an eigenvector is arbitrary,  $\text{EM}_1$  appears identically red. This corresponds to an average global mode that reflects

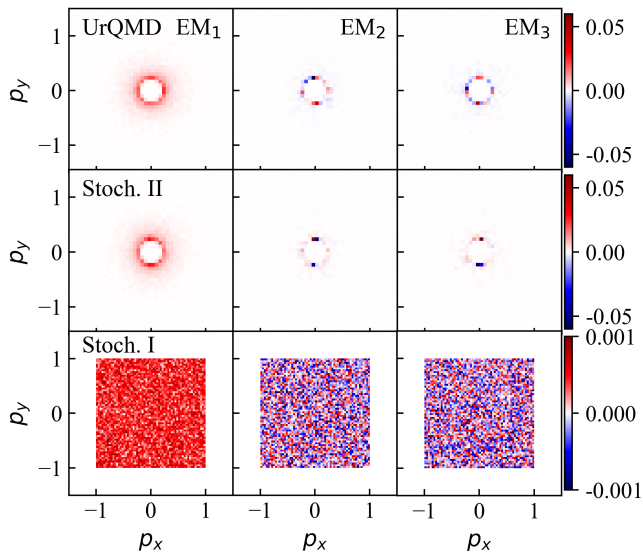


FIG. 1: (Color online) First three EMs (EM<sub>1</sub>, EM<sub>2</sub>, EM<sub>3</sub>) for UrQMD and for the two stochastic non-critical ensembles: Stoch. II and Stoch. I with and without kinetic constraints.

the overall radial momentum distribution with no internal cluster structure.

- EM<sub>2</sub> and EM<sub>3</sub> display *random red-blue fluctuations* with no stable patch-like or directional structure. They resemble noise patterns superimposed on the broad average global mode.
- The qualitative pattern of EM<sub>1</sub>–EM<sub>3</sub> is *very similar* among UrQMD, the uniform stochastic model, and the kinetic-constraint stochastic model.

These observations indicate that conventional correlations in UrQMD—including resonance decays, energy–momentum conservation, and collective flow—do not generate any coherent cluster-like EM patterns. The EMA thus filters out most non-critical correlations, leaving EMs that reflect only average global momentum shapes but no critical structure.

To quantify the eigenvalue hierarchy, Fig. 2 shows the cumulative weight  $C(m)$  for the three ensembles. In the uniform stochastic model I (without kinetic constraints),  $C(m)$  increases almost linearly with  $m$ , indicating that there is no preferred mode and the weights are distributed broadly over many EMs. By contrast, both the kinetic-constraint stochastic model II and UrQMD exhibit a rapid initial rise of  $C(m)$  followed by early saturation, reflecting the presence of a common global momentum shape that enhances a small number of leading non-critical modes.

The near agreement between UrQMD and the kinetic-constraint stochastic model II demonstrates that, in the absence of criticality, the EMA is predominantly sensitive to the global  $p_t$  and  $\phi$  distributions rather than to the detailed dynamical correlations of UrQMD. In particular,

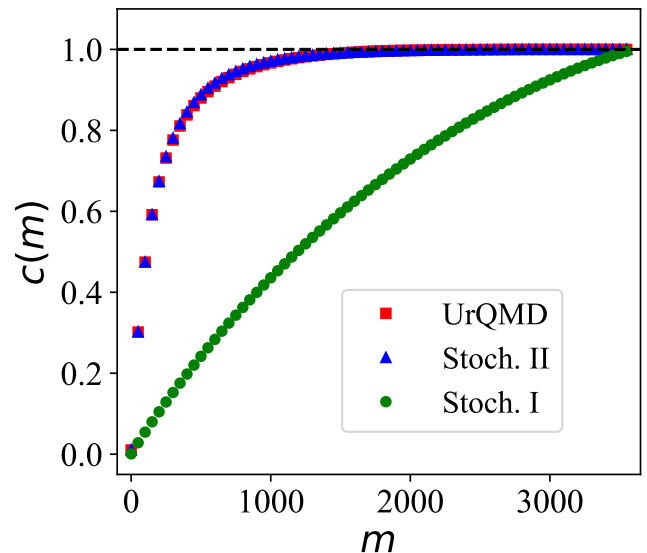


FIG. 2: (Color online) Cumulative weight  $C(m)$  for the UrQMD ensemble, the stochastic model II and I with and without kinetic constraints.

no cluster-like EM patterns emerge in any of the non-critical ensembles.

#### IV. EIGEN-MICROSTATES OF HYBRID MODELS

We now introduce critical fluctuations into the UrQMD baseline using a CMC model and examine how the EM patterns and eigenvalue spectra respond. The goal is to identify how critical cluster-like structures emerge in EMs as the critical fraction increases, and to compare event-level and particle-level embedding of criticality.

##### A. Critical Monte Carlo model

The CMC model [31, 32] is designed to generate critical momentum-space fluctuations through Lévy random walks. In each event, particle momenta are produced through successive steps of Lévy in the  $(p_x, p_y)$  plane [33, 34], leading to a scale-invariant fractal density characteristic of systems near a CP. The Lévy index controls the fractal dimension of the fluctuations, and the resulting events exhibit multi-scale clustering, voids, and long-range correlations.

Importantly, CMC does *not* impose global kinetic-shape distributions such as the Gamma  $p_t$  spectrum or flow-modulated azimuthal distributions used in the stochastic model II. Instead, its fluctuations arise from the fractal Lévy process itself, which encodes the essential physics of criticality.

## B. Construction of hybrid UrQMD+CMC samples

To investigate how EMA responds to critical fluctuations embedded in a realistic heavy-ion background, we construct hybrid event ensembles that combine UrQMD and CMC. We consider two physically distinct scenarios:

- **Replacement of event-level (fraction  $\alpha_e$ ).** A fraction  $\alpha_e$  of events in the UrQMD ensemble is completely replaced by CMC events. In this case, some events are purely non-critical (UrQMD) while others are fully critical (CMC). This scenario mimics a situation in which only a subset of heavy-ion collisions traverse the critical region in the QCD phase diagram.
- **Particle-level replacement (fraction  $\alpha_p$ ).** In each UrQMD event, a fraction  $\alpha_p$  of particles is replaced by particles drawn from a CMC event. This represents localized critical droplets embedded within non-critical events. To avoid distorting the UrQMD  $p_t$  spectrum, we impose a  $p_t$ -matching condition on each replacement:

$$|p_t^{\text{CMC}} - p_t^{\text{UrQMD}}| < 0.2 \text{ GeV}/c. \quad (8)$$

In both scenarios, the same acceptance cuts as in the UrQMD baseline are applied to the final hybrid samples. We then perform EMA on these hybrid ensembles with  $M = 20,000$  events for each choice of  $\alpha_e$  or  $\alpha_p$ .

## C. Emergence of critical cluster patterns in eigen-microstates

Figure 3 shows the first three EMs for hybrid ensembles constructed with event-level replacement (left columns) and particle-level replacement (right columns) in several critical fractions.

For **event-level replacement**, we observe:

- At  $\alpha_e = 0.1\%$ ,  $\text{EM}_1$  still resembles the UrQMD baseline pattern, while  $\text{EM}_2$  and  $\text{EM}_3$  begin to exhibit a weak separation of the red and blue regions, signaling the onset of a new collective mode associated with criticality.
- At  $\alpha_e = 0.8\%$ , clear patch- or cluster-like structures appear in all three leading EMs. These patterns break the approximate rotational symmetry seen in the non-critical baseline and exhibit localized regions of enhanced positive or negative fluctuation.
- At  $\alpha_e = 4\%$ , the cluster-like patterns in  $\text{EM}_1$ – $\text{EM}_3$  become strong and stable:  $\text{EM}_1$  is dominated by a coherent two-patch structure, while  $\text{EM}_2$  and  $\text{EM}_3$  show subleading but still well-organized patch-patterns.

For **particle-level replacement**, the emergence of cluster-like EM patterns is qualitatively similar but requires significantly larger critical fractions  $\alpha_p$ :

- At  $\alpha_p = 3\%$ ,  $\text{EM}_1$  remains close to the baseline pattern and  $\text{EM}_2$ ,  $\text{EM}_3$  appear in the embryonic form of a cluster-like pattern.
- At  $\alpha_p = 9\%$ , the development of cluster-like patterns is more visible in  $\text{EM}_1$  and  $\text{EM}_2$ .  $\text{EM}_3$  continues to be a baseline pattern; however, its weight gradually decreases, exhibiting a vanishing trend.
- At  $\alpha_p = 12\%$ , all three leading EMs exhibit clearly developed cluster-like patterns.

The comparison between event-level and particle-level replacement demonstrates that EMA is particularly sensitive to *coherent event-level criticality*: a very small fraction of fully critical events ( $\alpha_e \sim 0.1\%$ – $1\%$ ) already leave a visible imprint on the EM patterns. By contrast, localized critical droplets require substantially larger particle-level fractions ( $\alpha_p \gtrsim 9\%$ ) to produce comparable cluster structures. This difference reflects the fact that EMs are collective modes of the entire event ensemble and thus respond more strongly to coherent event-level structure than to local perturbations. However, the outlines of cluster-like patterns of particle-level replacement (right of Fig.3) are more clear and regular than those of event-level replacement (left of Fig.3).

These results provide important guidance for experimental searches: if criticality is realized only in a small subset of events at certain collision energies or centralities, its earliest signatures in EMA are expected to appear as the emergence and subsequent sharpening of cluster-like structures from a UrQMD background.

## D. Eigenvalue behavior and cumulants

Complementary information is provided by the eigenvalue hierarchy. Figure 4 shows the three largest weights  $w_1$ ,  $w_2$ ,  $w_3$  as a function of  $\alpha_e$  (event-level replacement) and  $\alpha_p$  (particle-level replacement), together with the corresponding cumulative weight  $C(m)$ .

For event-level replacement [Fig. 4(a)],  $w_1$  increases smoothly with  $\alpha_e$  and approaches a saturated value when  $\alpha_e \gtrsim 30\%$ . The subleading weights  $w_2$  and  $w_3$  also increase with  $\alpha_e$ , but  $w_3$  remains well separated from  $w_1$ , indicating the emergence of a dominant collective mode associated with the critical component. The associated cumulative weights  $C(m)$  in Fig. 4(b) show that, as  $\alpha_e$  increases, a smaller number of leading EMs account for most of the total weight:  $C(m)$  increases more dramatically and saturates earlier than that in the pure UrQMD baseline. This behavior reflects the increasingly prominent role of the critical collective mode as entire critical events are added.

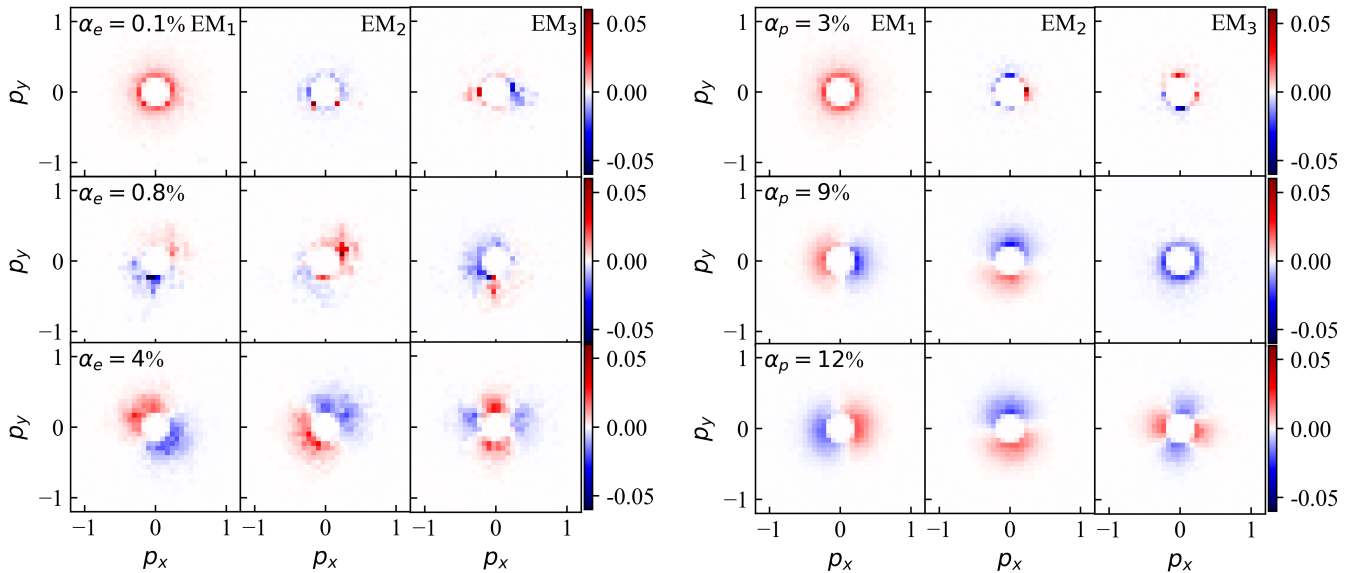


FIG. 3: (Color online) First three EMs for hybrid UrQMD+CMC ensembles constructed with event-level replacement (left columns) and particle-level replacement (right columns) for several critical fractions  $\alpha_e$  and  $\alpha_p$ .

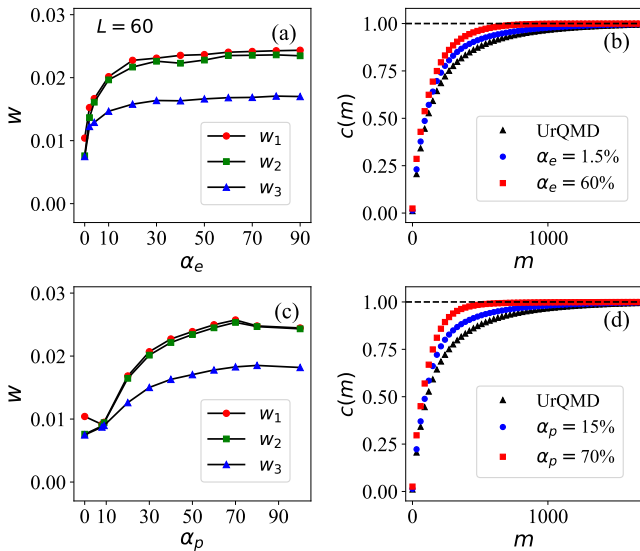


FIG. 4: (Color online) Top three eigenvalues  $w_1$ ,  $w_2$ ,  $w_3$  as functions of the critical fractions  $\alpha_e$  (event-level replacement) and  $\alpha_p$  (particle-level replacement), together with the corresponding cumulative weight  $C(m)$ .

For particle-level replacement [Fig. 4(c)],  $w_1$  displays a more complex behavior. At very small  $\alpha_p$ , it can exhibit a slight decrease, reflecting the disruption of the baseline mode by a small number of critical signal particles. Once the critical fraction becomes sufficiently large,  $w_1$  begins to increase and eventually saturates at large  $\alpha_p$ , analogous to an order parameter approaching its ordered-phase value. The corresponding cumulative weights  $C(m)$  in Fig. 4(d) show an analogous trend: with

increasing  $\alpha_p$  the rise of  $C(m)$  becomes steeper and saturation occurs at smaller  $m$ , indicating that a few leading EMs increasingly dominate the ensemble.

Taken together, these results underscore the role of  $w_1$  (or equivalently  $\lambda_1$ ) as an order-parameter-like quantity that measures the strength of the dominant collective mode, while the behavior of  $C(m)$  provides a complementary indication of how strongly the critical component controls the ensemble of events.

## V. FINITE-SIZE SCALING BEHAVIOR

A hallmark of critical phenomena is finite-size scaling. To further test the critical nature of the EM signatures, we examine how EM patterns and eigenvalue ratios behave on different scales  $L$  at fixed critical fractions. The scale  $L$  is represented by the number of divisions along one dimension.

Figure 5 presents the leading EMs for hybrid ensembles with  $\alpha_e = 4\%$  on three scales,  $L = 10, 40,$  and  $100$ . As  $L$  increases, the EM patterns become more dilute due to the finer binning. However, the underlying patch or cluster-like structures remain clearly visible and morphologically similar across scales: EM<sub>1</sub> and EM<sub>2</sub> exhibit two large patches while EM<sub>3</sub> shows more patches that are qualitatively self-similar for different  $L$ . This scale-invariant character of the patterns is consistent with the fractal nature of critical fluctuations.

Quantitatively, we analyze the ratio  $w_3/w_1$  as a function of  $\alpha_e$  and  $\alpha_p$  for  $L = 40, 60,$  and  $100$ , as shown in Fig. 6. At very small critical fractions, the three scales yield different values of  $w_3/w_1$ , reflecting significant finite-size effects and the dominance of non-critical

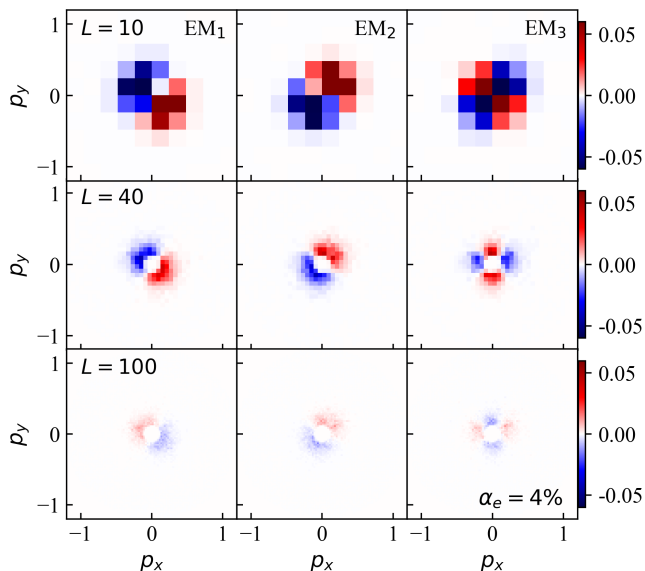


FIG. 5: (Color online) First three EMs at fixed  $\alpha_e = 4\%$  for three scales  $L = 10, 40, \text{ and } 100$ .

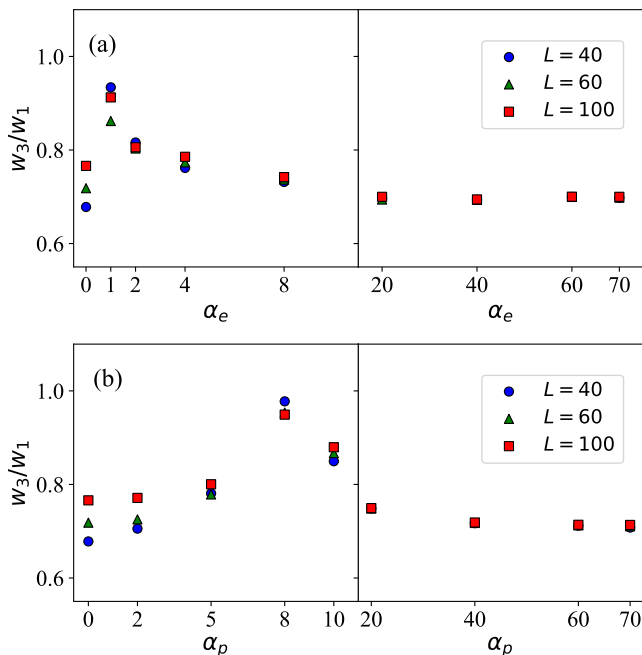


FIG. 6: (Color online) Ratio  $w_3/w_1$  as a function of  $\alpha_e$  and  $\alpha_p$  for scales  $L = 40, 60, \text{ and } 100$ .

fluctuations. As  $\alpha_e$  increases, the curves corresponding to different  $L$  move closer together and eventually overlap for  $\alpha_e \gtrsim 4\%$ , indicating a fixed-point-like behavior. A similar convergence is observed for the replacement of the particle-level at  $\alpha_p \gtrsim 9\%$ .

The fixed-point behavior of the eigenvalue ratio  $w_3/w_1$  in the same critical fractions strengthens the interpretation of EMA signatures as genuine indicators of critical-

ity. The scale invariance of the EMs pattern in Fig. 5 shows that the fractal nature of the critical fluctuations is captured by the EMs. Both pattern-level and scalar observables are consistent with finite-size scaling expectations.

## VI. SUMMARY AND CONCLUSIONS

In this work, we performed a detailed model study of the EMA to identify critical fluctuations in relativistic heavy-ion collisions. By analyzing UrQMD, stochastic reference ensembles, and hybrid UrQMD+CMC samples, we clarified the sensitivity of EMA to critical fluctuations and explored the self-similarity of EM and finite-size scaling properties of the eigenvalues.

We first showed that, for non-critical ensembles, the leading EMs and eigenvalue spectra are primarily determined by average global kinetic constraints (the  $p_t$  and  $\phi$  distributions), and that conventional correlations in UrQMD leave only little imprint in the EM patterns. EM<sub>1</sub> is essentially an average global mode, while EM<sub>2</sub> and EM<sub>3</sub> display random noise-like fluctuations, and no cluster-like structures are observed. The cumulative weights for UrQMD and the kinetic-constraint stochastic model are nearly identical and differ clearly from the uniform stochastic model, demonstrating that EMA acts as an efficient filter of non-critical background correlations.

We then embedded critical fluctuations using the CMC model and studied two hybrid scenarios: event-level replacement, in which entire UrQMD events are replaced by CMC events, and particle-level replacement, in which only fractions of particles in each event are replaced. We found that EM patterns are particularly sensitive to coherent event-level criticality: a very small fraction of fully critical events already reshape EM<sub>2</sub> and EM<sub>3</sub>, and modest  $\alpha_e$  yields robust cluster-like patterns in all leading EMs. Particle-level replacement produces qualitatively similar behavior but requires substantially larger critical fractions to achieve comparable cluster structures, reflecting the weaker coherence of local critical droplets.

The largest eigenvalue or weight  $w_1$  behaves as an order-parameter-like quantity in both hybrid scenarios, increasing and eventually saturating as the critical fraction grows. The cumulative weight  $C(m)$  saturates earlier in the presence of criticality, indicating that a small number of EMs dominate the ensemble. Finite-size scaling analyzes of EM patterns and of fixed-point behavior of the ratio  $w_3/w_1$  reveal at the same critical fractions, providing further evidence that EMA signatures reflect genuine critical scaling.

These results demonstrate that the eigen-microstate approach offers a new and background-independent framework for identifying critical behavior in event-by-event heavy-ion data. The methodology and signatures identified here provide direct guidance for applying EMA to RHIC BES II data and to future experiments at FAIR, NICA, and HIRFL-CSR. In particular, scanning collision

energy and centrality for the onset of cluster-like EM patterns and fixed-point-like behavior in eigenvalue ratios may prove to be a promising strategy for locating the QCD critical point.

### Acknowledgments

This research was funded by the China National Key Research and Development Program, Grant

No. 2024YFA1610700, and 2022YFA1604900, the National Natural Science Foundation of China, Grant Nos. 12275102, 12135003, 12205058, and the Natural Science Foundation of Guangxi, Grant No. 2023GXNSFBA026043.

- 
- [1] A. Bzdak, S. Esumi, V. Koch, J. F. Liao, M. Stephanov, and N. Xu, *Physics Reports* **853**, 1 (2020).
- [2] Y. Aoki, G. Endrodi, Z. Fodor, S. D. Katz, and K. K. Szabo, *Nature* **443**, 675 (2006).
- [3] M. Asakawa and K. Yazaki, *Nucl. Phys. A* **504**, 668 (1989).
- [4] J. Berges and K. Rajagopal, *Nucl. Phys. B* **538**, 215 (1999).
- [5] M. A. Stephanov, K. Rajagopal, and E. V. Shuryak, *Phys. Rev. D* **60**, 114028 (1999).
- [6] M. A. Stephanov, *Phys. Rev. Lett.* **102**, 032301 (2009).
- [7] STAR Note 0598: BES-II white paper, <https://drupal.star.bnl.gov/STAR/starnote/public/sn0598> (2014).
- [8] S. Ejiri, F. Karsch, and K. Redlich, *Phys. Lett. B* **633**, 275 (2006).
- [9] A. Bialas and R. Peschanski, *Nucl. Phys. B* **273**, 703 (1986).
- [10] Y. Wu and L. Liu, *Phys. Rev. Lett.* **70**, 3197 (1993).
- [11] A. Bzdak, V. Koch, and N. Strodthoff, *Phys. Rev. C* **95**, 054906 (2017).
- [12] B. E. Aboona *et al.* (STAR), *Phys. Rev. Lett.* **135**, 142301 (2025).
- [13] M. Nahrgang, M. Bluhm, T. Schafer, and S. A. Bass, *Phys. Rev. D* **99**, 116015 (2019).
- [14] S. Wu, Z. Wu, and H. Song, *Phys. Rev. C* **99**, 064902 (2019).
- [15] K. Rajagopal, G. W. Ridgway, R. Weller, and Y. Yin, *Phys. Rev. D* **102**, 094025 (2020).
- [16] X. Li, M. Xu, Y. Zhang, Z. Li, Y. Zhou, J. Fu, and Y. Wu, *Phys. Rev. C* **105**, 064904 (2022).
- [17] X. Li, R. Guo, M. Xu, J. Fu, L. Chen, Y. Zhou, and Y. Wu, *Phys. Rev. E* **111**, 064115 (2025).
- [18] L. Chen, Y. Zhao, Y. Cheng, G. Wang, Z. Li, and Y. Wu, *Phys. Rev. C* **109**, 034911 (2024).
- [19] A. Bzdak and V. Koch, *Phys. Rev. C* **100**, 051902(R) (2019).
- [20] G. Hu, T. Liu, M. Liu, W. Chen, and X. Chen, *Sci. China-Phys. Mech. Astron.* **62**, 990511 (2019).
- [21] Y. Sun, G. Hu, Y. Zhang, B. Lu, Z. Lu, J. Fan, X. Li, Q. Deng, and X. Chen, *Commun. Theor. Phys.* **73**, 065603 (2021).
- [22] X. Li, T. Xue, Y. Sun, J. Fan, H. Li, M. Liu, Z. Han, Z. Di, and X. Chen, *Chin. Phys. B* **30**, 128703 (2021).
- [23] X. Li, X. Xiang, T. Xue, L. Wang, and X. Chen, *Sci. China-Phys. Mech. Astron.* **67**, 110511 (2024).
- [24] T. Liu, G. Hu, J. Dong, J. Fan, M. Liu, and X. Chen, *Chinese Phys. Lett.* **39**, 080503 (2022).
- [25] L. Wang, *Phys. Rev. B* **94**, 195105 (2016).
- [26] R. Guo, J. Wu, M. Xu, X. Chen, Z. Li, Z. Yin, and Y. Wu, Eigen-microstate signatures of criticality in relativistic heavy-ion collisions (2025), arXiv:2510.20336 [hep-ph] .
- [27] L. P. Pitaevskii and S. Stringari, *Bose-Einstein Condensation* (Clarendon Press, Oxford, 2003).
- [28] S. A. Bass *et al.*, *Prog. Part. Nucl. Phys.* **41**, 255 (1998).
- [29] M. Bleicher *et al.*, *J. Phys. G* **25**, 1859 (1999).
- [30] M. Abdulhamid *et al.* (STAR), *Phys. Lett. B* **845**, 138165 (2023).
- [31] N. G. Antoniou, F. K. Diakonou, A. S. Kapoyannis, and K. S. Kousouris, *Phys. Rev. Lett.* **97**, 032002 (2006).
- [32] N. G. Antoniou, Y. F. Contoyiannis, F. K. Diakonou, A. J. Karanikas, and C. N. Ktorides, *Nucl. Phys. A* **693**, 799 (2001).
- [33] J. Wu, Z. Li, X. Luo, M. Xu, and Y. Wu, *Phys. Rev. C* **106**, 054905 (2022).
- [34] R. Wang, C. Qiu, C. Hu, Z. Li, and Y. Wu, *Phys. Lett. B* **864**, 139405 (2025).